JMEPEG (2015) 24:1379–1389
DOI: 10.1007/s11665-015-1400-x

1059-9495/$19.00

Effect of CeO_2 on Cyclic Hot-Corrosion Behavior of Detonation-Gun Sprayed Cr_3C_2-NiCr Coatings on Ni-Based Superalloy

Sekar Saladi, Jyoti Menghani, and Satya Prakash

(Submitted October 10, 2014; in revised form December 23, 2014; published online January 24, 2015)

The hot-corrosion behavior of detonation-gun sprayed Cr_3C_2-NiCr coatings with and without 0.4 wt.% CeO_2 additive on Ni-based superalloy inconel-718 is comparatively discussed in the present study. Hot-corrosion studies were carried out at 900 °C for 100 cycles in Na_2SO_4-60%V_2O_5 molten salt environment under cyclic heating and cooling conditions on bare and coated superalloys. The thermo-gravimetric technique was used to establish kinetics of hot-corrosion. XRD, FESEM/EDAX, and EDX mapping techniques were used to analyze the corrosion products of bare and coated samples. The results indicate that Cr_3C_2-NiCr-CeO_2-coated superalloy showed better hot-corrosion resistance as compared to bare and Cr_3C_2-NiCr-coated superalloys. The addition of CeO_2 has improved micro-hardness, porosity, and surface roughness values of Cr_3C_2-NiCr-CeO_2 coating. The overall weight gain and parabolic rate constant of Cr_3C_2-NiCr-CeO_2-coated superalloy were found to be lowest in the present study signifying that the addition of CeO_2 in Cr_3C_2-NiCr powder has contributed to the development of adherent and dense oxide scale on the coating at elevated temperature.

Keywords CeO_2, coatings, Cr_3C_2-NiCr, detonation-gun, hot-corrosion, superalloys

1. Introduction

Rapid degradation of hot section components in gas and steam turbines, boilers, industrial waste incinerators etc., is mainly due to hot-corrosion, oxidation, and erosion (Ref 1). Hot-corrosion occurs as a result of attack by fuel and/or ash compounds of sodium, vanadium, sulfur, and chlorine that are present in the fuels used for combustion (Ref 2, 3). As a consequence, the material is consumed at unpredictably rapid rate due to the formation of un-protective oxides and the load carrying capability of the components is reduced, leading to its catastrophic failure (Ref 3, 4). Nickel-based superalloy Inconel-718 (In-718) is extensively used for high-temperature parts of gas and steam turbines as it has excellent mechanical properties such as tensile strength, creep resistance, and low-cycle fatigue strength. The alloy currently accounts for 45% of wrought nickel-based superalloy production (Ref 5, 6). Although In-718 possesses adequate strength at the turbine operating temperatures, it often lacks resistance against the hot-corrosion environment (Ref 6, 7).

In the combustion system, sodium and sulfur react with each other to form Na_2SO_4 (m.p 884 °C), while vanadium reacts with oxygen to form V_2O_5 (m.p 670 °C) (Ref 7). Na_2SO_4 and V_2O_5 further react at high temperature to form low melting (m.p below 630 °C) sodium vanadates that are highly corrosive (Ref 8). A mixture of Na_2SO_4 and V_2O_5 in the ratio of 40:60 wt.% is reported to be a very aggressive environment for hot-corrosion to occur in superalloys (Ref 9). When the operating temperature exceeds the melting point of these compounds, they start slowly depositing on the turbine blades; consequently corrosion rate rapidly increases due to faster transport phenomena in liquid phase, leading to catastrophic failure (Ref 7). Further, vanadium compounds are good oxidation catalysts; they transport oxygen and other corrosive species from the combustion atmosphere to the metal surface and cause severe corrosion. Thus, in order to improve the efficiency of a gas turbine engine significantly, the hot-corrosion resistance of superalloys is as important as its high temperature strength (Ref 10). Currently, one of the effective solutions to above problem is to coat the alloy with hot-corrosion resistant protective coatings using various surface-treatment techniques (Ref 1, 8, 11, 12).

Chromium carbide-nickel chromium (Cr_3C_2-NiCr) cermet coating is widely used in gas and steam turbines, aero-engines, oil-refining industry, heat treatment rolls, and coal burning boiler tubes (Ref 13-15). It is one of the most extensively researched coatings (Ref 16, 17). These coatings consist of hard carbide phase Cr_3C_2 which provides good wear resistance and tough metal matrix phase NiCr providing hot-corrosion and oxidation resistance in high-temperature environments. The Cr_3C_2-NiCr coatings are widely produced using HVOF spraying process, as it produces good quality coatings (Ref 18). However, the coatings deposited using Detonation-gun (D-gun) spray process also exhibit low porosity, higher bond strength, and hardness with fine gain structure. D-gun offers highest velocity (800-1200 ms^{-1}) among thermal spray processes, due to which there is minimum decomposition of the feed powder during the coating process (Ref 19). Senderowski et al. (Ref 20-25) have reported that FeAl inter-metallic coatings deposited using D-gun technology were characterized by low

Sekar Saladi and **Jyoti Menghani**, SVNIT - Mechanical Engineering, Dumas Rd, Ichchhanath, Surat, Gujarat 395007, India; and **Satya Prakash**, Department of Metallurgical and Materials Engineering, Indian Institute of Technology, Roorkee, Roorkee, Uttarakhand, India. Contact e-mail: sekarpmt.iitr@rediffmail.com.

porosity, high temperature corrosion and oxidation resistance, reduced negative gradients of stress and temperature influencing the substrate and increasing adhesion strength. Sundarajan et al. (Ref 26) and Kamal et al. (Ref 10) have reported that the porosity values of D-gun sprayed coatings are less than that of the coatings deposited by other thermal spray techniques.

However, despite the effectiveness of the coating composition, the lifetime of components operating in high-temperature degrading environments are limited by the lifetime of the protective coatings (Ref 27). As no alloy is immune to hot-corrosion for infinitely long period, any improvement in the performance of Cr_3C_2-NiCr coatings will be of great importance to the field of surface engineering. Recent studies have shown that by adding small amounts of rare earth compounds, the surface properties such as oxidation, corrosion, and wear resistance of various coatings can be improved due to the improved hardness, toughness, bond strength, and thermal shock resistance of the coating materials (Ref 28). Wang et al. were the first to introduce rare earth elements to improve wear and corrosion resistance of protective coatings (Ref 29-32). Mahesh et al. (Ref 33) reported that addition of 0.4 wt.% CeO_2 has improved oxidation resistance of high-velocity oxy fuel (HVOF)-sprayed NiCrAlY coatings on superalloys at elevated temperature. Kamal et al. (Ref 32, 34) investigated the microstructure, mechanical properties, and hot-corrosion resistance of D-gun sprayed CeO_2-added NiCrAlY coatings and concluded that the addition of ceria resulted in forming finer microstructure with improved hot-corrosion resistance. Zhang et al. (Ref 18) evaluated the tribological properties of La_2O_3 and CeO_2-added Cr_3C_2-NiCr coatings. They inferred that the addition of rare earth oxides to the coatings leads to the improvement of surface roughness, micro-hardness, and decrease of friction coefficient. Gui-hua et al. (Ref 35) studied the effect of rare earth yttrium (Y) on cyclic oxidation behavior of NiAl-Al_2O_3 and reported that with the addition of Y, the mass gain during oxidation is greatly reduced. It also changed the morphology of scale, while eliminating cracking and spallation of the oxide scale. Xu et al. have reported that ceria-added rare earth zirconates exhibited the best performance for hot-corrosion resistance in comparison with coatings without ceria (Ref 36). But, there is a very little literature available on the effect of CeO_2 on the cyclic hot-corrosion behavior of D-gun sprayed Cr_3C_2-NiCr coatings on superalloys in different aggressive environments. Therefore, the present study investigates the cyclic hot-corrosion behavior of D-gun sprayed Cr_3C_2-NiCr-CeO_2 coatings on nickel-based superalloy In-718 in Na_2SO_4-60%V_2O_5 molten salt environment at 900 °C. The thermo-gravimetric technique was used to establish kinetics of hot-corrosion. X-ray diffraction, FESEM/EDAX, and EDX mapping techniques were used to analyze the corrosion products of bare and coated superalloys.

2. Experimental Procedure

2.1 Substrate Material and Coating Formulation

Nickel-based superalloy In-718 used in the present study was procured from Narendra Steels, Mumbai, (India), in rolled sheet form. The nominal chemical composition (wt.%) of the substrate material is given in Table 1. Each specimen measuring approximately 20 mm × 15 mm × 5 mm was cut from the rolled sheet. The specimen were polished and grit blasted (grit 45) with alumina prior to D-gun coating. Commercially available 75 wt.%Cr_3C_2-25 wt.%(Ni-20Cr) (AMPERIT®/584.072-H.C. Starck) powder designated as Cr_3C_2-NiCr is used in this study. A mixture of CeO_2 (0.4 wt.%) with 99.99% purity and Cr_3C_2-NiCr powder was dry-ball milled in a conventional rotating ball mill with stainless steel balls as a milling/grinding medium for 8 h to obtain homogenous blend of Cr_3C_2-NiCr and CeO_2 powders (designated as Cr_3C_2-NiCr-CeO_2) for the deposition of coatings (Fig. 1). D-gun (Model: Awaaz) process was used to apply coatings on all six sides of the superalloy at SVX Powder M Surface Engineering Pvt. Ltd, New Delhi (India). The spray parameters used during coating deposition are given in Table 2.

2.2 Characterization of Coatings

Bruker AXS D-8 Advance diffractometer with Cu Kα radiation was used for the phase identification in the XRD analysis of the samples. The surface and cross-sectional analysis of the samples were analyzed using field emission scanning electron microscope (FESEM, FEI, Quanta 200F Company) with EDAX Genesis software attachment. The micro-hardness of the coating along the cross section of the coated superalloys as a function of distance from the coating-substrate interface was measured by using a Leitz miniload 2 (Germany) hardness tester. A load of 15 g (147.1 mN) was provided to the needle for penetration, and the hardness value was calculated from the relation $Hv = 1854.4 \times F/d^2$ (where F is load in grams and d is the mean penetrated diameter in micrometer). The cohesive and adhesive porosity values were assessed by photomicrograph quantitative analysis carried out with JEOL-JSM 5610LV (SEM). The cohesive porosity values were calculated based on the ratio of the sum of pore surfaces to the total surface of the specimen. On the other hand, the adhesive porosity (in the coating substrate joint) was defined as a ratio of the sum of the lengths of pore chords to the length of measuring length on the specimen surface (Ref 21, 37). Surface roughness tester (Mitutoyo SJ-201, Japan) was used to measure the surface roughness (Ra) of the as-sprayed coatings at five different locations. The centre line average (CLA) method was used to obtain the Ra values.

2.3 Hot-Corrosion Tests in Molten Salt Environment

Hot-corrosion studies were performed in cyclic conditions on bare, Cr_3C_2-NiCr and Cr_3C_2-NiCr-CeO_2-coated In-718 superalloy substrate in Na_2SO_4-60%V_2O_5 molten salt environment at 900 °C for 100 cycles. Each cycle consists of 1 h heating at 900 °C followed by 20 min cooling at room temperature. The cyclic hot-corrosion studies create the severest conditions for testing; which simulate the conditions prevailing in actual service environment of the superalloy components, where breakdown/shutdown occurs frequently. A coating of uniform thickness with 3-5 mg/cm^2 of Na_2SO_4-60% V_2O_5 salt mixed in distilled water was applied with the help of camel hair brush on samples preheated in an oven maintained at 250 °C for 2 h. The preheating of samples was found necessary for the proper adhesion of the salt layer. The salt-coated specimens were then kept in an oven maintained at 150 °C for 2 h for complete drying and proper adhesion of the salt. Subsequently, the specimen was placed in alumina boat and weighed using micro balance (model BSA224S-CW, Sartorius) with a sensitivity of 0.1 mg, before exposing to hot-corrosion tests. The spalled scale was also included at the time of weight

Table 1 Chemical composition of superalloy Inconel-718

	Chemical composition (wt.%)										
Inconel-718	Ni	Fe	Cr	Ti	Al	Mo	Mn	Si	Cu	C	Nb
	53.88	17.68	17.87	1.2	0.55	2.92	0.14	0.24	0.11	0.03	4.97

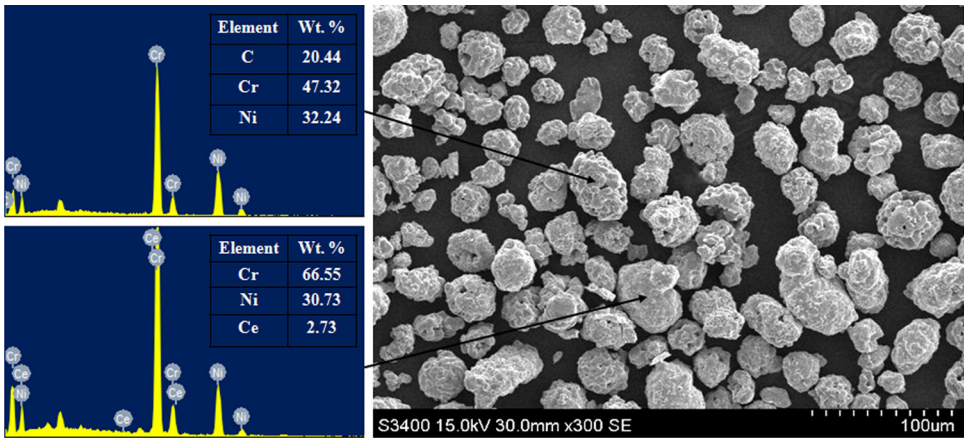

Fig. 1 SEM image showing the morphology of Cr_3C_2-NiCr-CeO_2 powder blend

Table 2 Spray parameters used to deposit Cr_3C_2-NiCr and Cr_3C_2-NiCr-CeO_2 coatings

Spray parameters	
Acetylene (C_2H_2) flow rate	2.32 m^3 h^{-1}
Oxygen (O_2) flow rate	2.64 m^3 h^{-1}
Carrier gas (N_2) flow rate	0.96 m^3 h^{-1}
Frequency of shots	3 shots s^{-1}
Spot size (diameter)	20 mm
Spraying distance from nozzle	165 mm
Powder flow rate	1-2 g/shot
Length of the barrel	1350 mm

change measurement to determine total rate of corrosion. The kinetics of corrosion was analyzed from the results of weight change measurements. XRD, FESEM/EDAX, and EDX mapping techniques were used to analyze the corrosion products.

3. Results

3.1 General Features of As-Sprayed Coatings Prior to Hot-Corrosion Studies

The cross-sectional morphology of as-sprayed Cr_3C_2-NiCr and Cr_3C_2-NiCr-CeO_2 coatings deposited using D-gun process is shown in Fig. 2. It is observed that Cr_3C_2-NiCr-CeO_2 coating shows uniform and dense microstructure, with very little porosity (Fig. 2b) as compared to Cr_3C_2-NiCr coating. Both coatings show Cr_3C_2-rich dark gray regions and NiCr-rich light gray regions.

In gas and steam turbines, the protective coatings may have to encounter the problem of erosion-corrosion degradation. Micro-hardness is an important property of the coatings, as hard coatings provide better erosion and wear resistance than soft coatings. Porosity is also one of the important parameters to be measured for the coatings, as it affects the corrosion resistance by providing easy access to corrosive species to penetrate through it and reach the substrate material. The coating thickness was measured from the back-scattered electron images (BSEI) collected with SEM for Cr_3C_2-NiCr and Cr_3C_2-NiCr-CeO_2 coatings. Table 3 presents the micro-hardness, porosity, coating thickness, and surface roughness values of D-gun sprayed coatings.

3.2 Effect of Cyclic Hot-Corrosion Studies on Bare and Coated Superalloys

3.2.1 Visual Observations. The photographs of bare, Cr_3C_2-NiCr and Cr_3C_2-NiCr-CeO_2-coated superalloys subjected to cyclic hot-corrosion studies for 100 cycles at 900 °C in Na_2SO_4-60% V_2O_5 environment are shown in Fig. 3. The surface scale formed on the bare superalloy was initially dark gray in color and later turned to dark brown during the course of the study. By the end of 100 cycles, a complete layer of oxide scale got exfoliated from the bare superalloy surface (Fig. 3a). On the other hand, the scale formed on Cr_3C_2-NiCr-coated In-718 was dark gray up to 15 cycles. During further cycles, the color of the scale turned to dark green and after 23rd cycle cracks started to appear mainly near the edges of the coated superalloy along with slight spalling of the oxide scale. By the end of 100 cycles, more cracks and spalling of oxide scale was observed (Fig. 3b). In case of Cr_3C_2-NiCr-CeO_2-coated In-718, the scale formed was initially dark gray (up to 18th cycle). After the end of 25th cycle, slight micro-spalling of the oxide scale in the form of powder was observed, this continued till the end of 100 cycles. No cracks were observed on the oxide scale formed on the surface of the Cr_3C_2-NiCr-CeO_2-coated superalloy (Fig. 3c).

3.2.2 Corrosion Kinetics in Molten Salt Environment. The Fig. 4(a) shows the weight gain per unit area versus number of cycles plot for the bare, Cr_3C_2-NiCr and Cr_3C_2-NiCr-CeO_2-coated

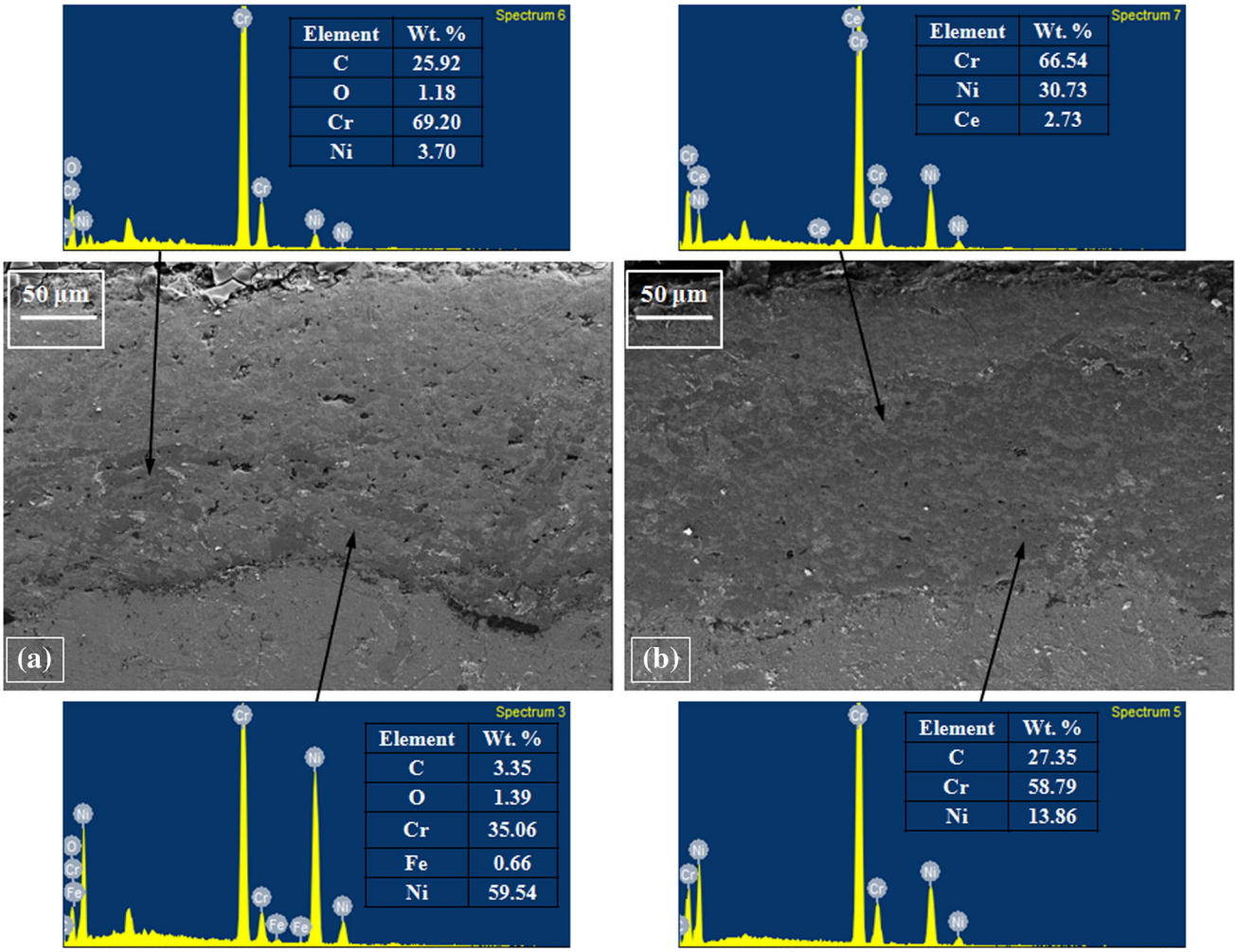

Fig. 2 SEM micrographs showing the cross-sectional morphology of D-gun sprayed (a) Cr_3C_2-NiCr and (b) Cr_3C_2-NiCr-CeO_2 coatings

Table 3 Micro-hardness, porosity, coating thickness, and surface roughness values of the coatings

	Average values				
		Porosity (%)			
Coating	Micro-hardness (Hv)	K_h	A_d	Thickness (µm)	Surface roughness (Ra, µm)
Cr_3C_2-NiCr	872	1.2	1.1	200	4.1
Cr_3C_2-NiCr-CeO_2	955	0.6	0.4	195	3.7

K_h cohesive porosity, A_d adhesive porosity

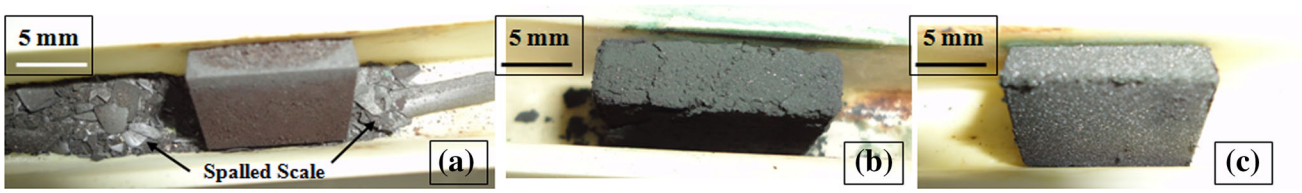

Fig. 3 Photographs of (a) bare (b) Cr_3C_2-NiCr and (c) Cr_3C_2-NiCr-CeO_2-coated superalloys subjected to hot-corrosion studies at 900 °C for 100 cycles

superalloys subjected to hot-corrosion in Na_2SO_4-60% V_2O_5 salt mixture at 900 °C for 100 cycles. The bare superalloys showed large weight gain up to 30 cycles, while the oxide scale formed on the surface of the bare superalloy was intact without any spallation. But, at the end of 31st cycle intense spalling of oxide scale had started and continued till the end of 100 cycles. Due to spalling, corrosion products started to fall outside the alumina boat and it became difficult to monitor the actual weight gain after 30 cycles. The bare superalloy nearly followed parabolic rate law up to 30 cycles and deviated from it during subsequent cycles (Fig. 4). In case of Cr_3C_2-NiCr and Cr_3C_2-NiCr-CeO_2-coated superalloys, the weight gain was relatively higher during initial 20 cycles and thereafter it was nearly gradual. Both Cr_3C_2-NiCr and Cr_3C_2-NiCr-CeO_2 coatings nearly followed parabolic rate law during the entire study. The (weight gain/area)^2 versus number of cycles data are plotted to show conformance with the parabolic rate law (Fig. 4b). The parabolic rate constant K_p was calculated by a linear least-square algorithm to a function in the form of $(\Delta W/A)^2 = K_p t$, where $\Delta W/A$ is the weight gain per unit surface area (mg/cm^2), t is the corrosion time in seconds. The parabolic rate constants (K_p in 10^{-10} g^2 cm^{-4} s^{-1}) for bare (Up to 30 cycles) was found to be 13.1, while for Cr_3C_2-NiCr and Cr_3C_2-NiCr-CeO_2-coated (up to 100 cycles) superalloys, it was found to be 13.7 and 6.7, respectively.

3.2.3 X-Ray Diffraction Analysis. The X-ray diffraction patterns of surface oxide scale of bare, Cr_3C_2-NiCr and Cr_3C_2-NiCr-CeO_2-coated superalloys after cyclic hot-corrosion studies are shown in Fig. 5. The main phases identified in case of bare superalloy were Cr_2O_3, Fe_2O_3, NiO, $NiVO_3$, $NiFe_2O_4$, $NiCr_2O_4$, and TiO_2. On the other hand Cr_3C_2-NiCr and Cr_3C_2-NiCr-CeO_2-coated superalloys showed all the above phases except $NiVO_3$ and TiO_2 along with the presence of Cr_3C_2 and $Cr_{23}C_6$ phases. An additional minor phase CeO_2 was observed in case of Cr_3C_2-NiCr-CeO_2-coated superalloy.

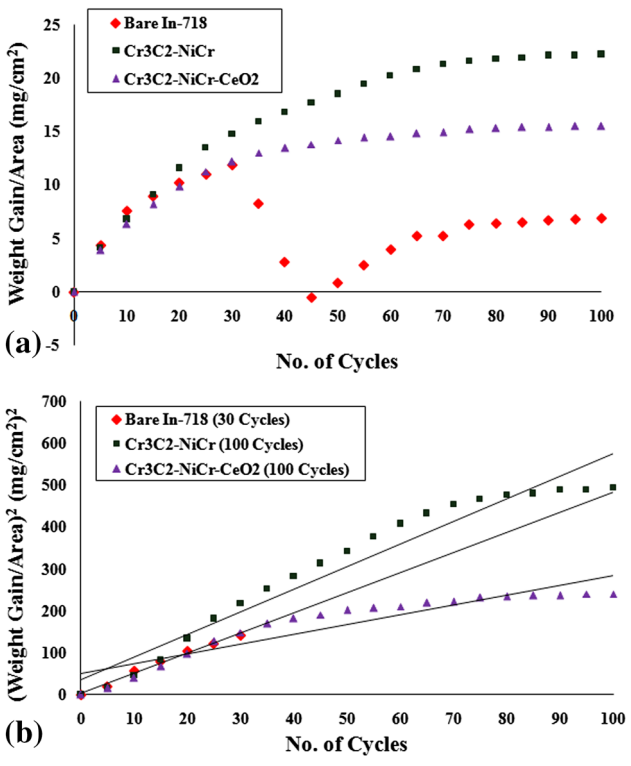

Fig. 4 (a) Weight gain/area vs. Number of cycles plot and (b) (weight gain/area)^2 vs. Number of cycles plot for bare, Cr_3C_2-NiCr and Cr_3C_2-NiCr-CeO_2-coated superalloys subjected to hot-corrosion studies at 900 °C for 100 cycles

3.2.4 Surface EDAX Analysis of the Oxide Scale. Figure 6 shows SEM micrographs with EDAX spectrum at selected points of interest on the surface of the bare, Cr_3C_2-NiCr and Cr_3C_2-NiCr-CeO_2-coated superalloys after cyclic hot-corrosion studies for 100 cycles. The surface scale formed on the bare superalloy is spongy in nature in some areas, with numerous micro-cracks (Fig. 6a). The main phases observed by EDAX analysis of the surface scale of bare superalloy are Cr_2O_3, Fe_2O_3, and NiO phases along with small amounts of Al_2O_3, TiO_2, and Nb_2O_5. In case of Cr_3C_2-NiCr and Cr_3C_2-NiCr-CeO_2 coatings, the main phases identified were Cr_2O_3, NiO and Fe_2O_3. Small pieces of spalled scale loosely attached to the surface were observed (Fig. 6b and c). An additional phase CeO_2 was observed in Cr_3C_2-NiCr-CeO_2 coating.

3.2.5 Cross-Sectional EDAX Analysis of Oxide Scale. The bare, Cr_3C_2-NiCr and Cr_3C_2-NiCr-CeO_2-coated superalloys subjected to hot-corrosion were cut along the cross section and mounted in epoxy resin, mirror polished and gold coated to study the cross-sectional details using FESEM/EDAX analysis. Analysis of top scale of the bare superalloy (Fig. 7a) shows mainly the presence of Cr, O, Fe, and Ni (point 1). The concentration of Cr and O increases while that of Fe and Ni decreases in the sub scale region (point 2-3). The concentration of O decreases at points 4-6 and small amount of sulfur (1.23%) is present at point 5. Points 6-8 show the composition of substrate material. On the other hand, analysis of top scale of Cr_3C_2-NiCr-coated superalloy (Fig. 7b) shows mainly the presence of Cr and O (points 1-2). The coating shows Ni-rich light gray (point 3) and Cr, C-rich dark gray regions (points 4-5). Oxygen has penetrated into the coating (points 1-5). Points 6 and 8 give the composition of the substrate material, while point 7 shows mainly the presence of Cr and O. Some amount of Fe has diffused from the substrate material into the coating (points 3-6). In case of Cr_3C_2-NiCr-CeO_2-coated superalloy (Fig. 7c), the top scale (points 1-3) shows mainly the presence of Cr along with O, Ni, C, and small amount of Ce (0.5 to 2.7%). The coating also shows Ni-rich light gray (point 4) and Cr, C-rich dark gray regions (points 5). The oxygen concentration is negligible in subscale region (points 4-6). Point 7 shows mainly the presence of Cr and O. Small amount of Fe has diffused into the coating (points 5-6). Point 8 shows the composition of substrate material.

3.2.6 EDX Mapping of Different Elements. The EDX mapping of Cr_3C_2-NiCr and Cr_3C_2-NiCr-CeO_2-coated superalloys (Fig. 8) shows that the splats mainly consist of Cr, Ni, O, and C, whereby indicating the formation of Cr- and Ni-rich oxides, along with chromium carbides. Ni-rich splats are found mostly at places where Cr is depleted. The concentration of O is high and that of C is less in the top scale as compared to subscale region. Fe, Mo, and Nb have diffused into the coating from the substrate material. A thin layer (few microns) of Cr and O co-exist underneath the Cr_3C_2-NiCr coating-substrate interface, showing that the O has penetrated the substrate material. In case of Cr_3C_2-NiCr-CeO_2 coating, it was observed that most of the Ni-rich splats in the subscale are un-oxidized indicating the as-sprayed nature of the coating. Cerium was found mainly near the inter-splat regions of Cr_3C_2-NiCr-CeO_2 coating.

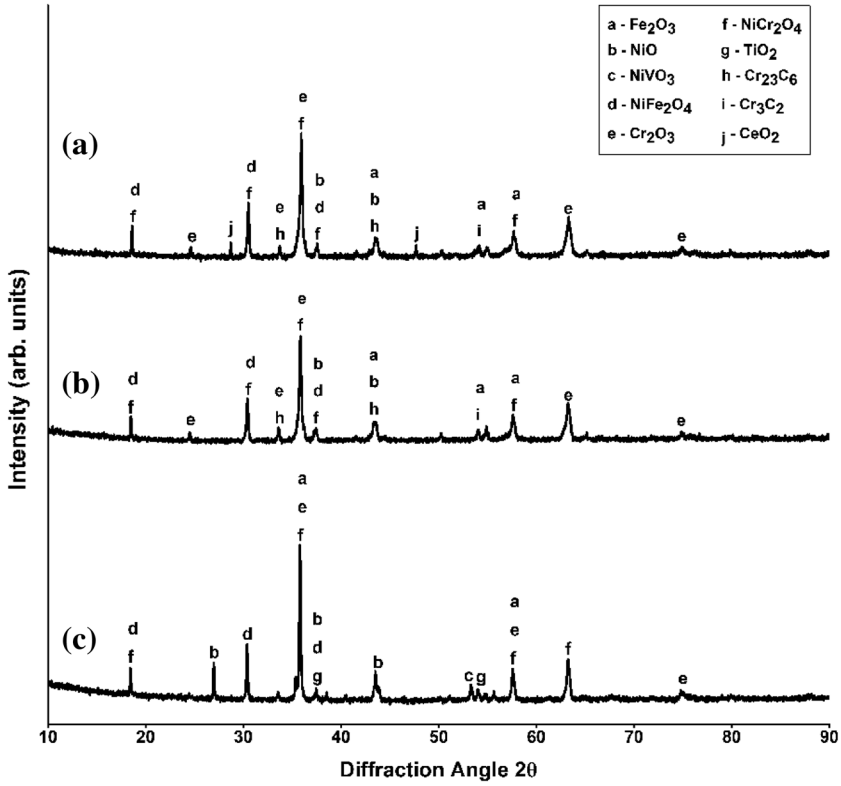

Fig. 5 X-Ray diffraction pattern of (a) bare (b) Cr_3C_2-NiCr and (c) Cr_3C_2-NiCr-CeO_2-coated superalloys subjected to hot-corrosion studies at 900 °C for 100 cycles

4. Discussion

The D-gun spray process can be successfully used to deposit Cr_3C_2-NiCr-CeO_2 coating. The SEM micrographs of Cr_3C_2-NiCr and Cr_3C_2-NiCr-CeO_2 coatings shown in Fig. 2 are dense, uniform and crack free. The D-gun sprayed Cr_3C_2-NiCr-CeO_2 coating has better micro-hardness, porosity, and surface roughness values as compared to Cr_3C_2-NiCr coating (Table 3). It has been reported by many researchers that addition of CeO_2 improves wetting of the surface by the coating material leading to better coating adhesion, thereby improving the micro-hardness and porosity values of the coating and in addition CeO_2 being surface-active element easily reacts with oxygen forming stable rare earth oxide compound at melting state. During the process of crystallization, CeO_2 can increase the amount of crystal nuclei and limit the growth of grain size, thus the microstructure of the coatings can be refined, leading to the improvement of surface morphology (Ref 18, 31, 32, 38, 39).

The weight change data for bare and coated superalloys after hot-corrosion studies are shown in Fig. 4. The weight gained by bare superalloy is higher than the coated superalloys. The weight gain of bare superalloy could not be monitored after 30 cycles, due to intense spalling of the oxide scale. Similar observations were also made by Kamal et al. (Ref 10) during hot-corrosion study on In-718. The Cr_3C_2-NiCr-CeO_2 coating showed least weight gain amongst coated samples. The cumulative weight gain at the end of 100 cycles for Cr_3C_2-NiCr and Cr_3C_2-NiCr-CeO_2 was found to be 22.2 and 15.5 mg cm^{-2}, respectively. It was found that the overall weight gain of Cr_3C_2-NiCr-CeO_2 coating is 30.2% less in comparison to that of Cr_3C_2-NiCr-coated superalloy. The parabolic rate constants (K_p in 10^{-10} g^2 cm^{-4} s^{-1}) is least for Cr_3C_2-NiCr-CeO_2 coating as compared to that of bare and Cr_3C_2-NiCr-coated superalloy thereby indicating better resistance to hot-corrosion in the given environment at 900 °C. Small deviation from the parabolic rate law may be due to the formation of in-homogeneous oxides such as Cr_2O_3 and NiO during oxidation process. Mahesh et al. (Ref 40) and Choi et al. (Ref 41) also reported the formation of similar oxides during their study. In addition, the Cr_3C_2-NiCr-CeO_2 coating showed no cracking with very little spallation of oxide scale as compared to bare and Cr_3C_2-NiCr coating. This may be due to grain refinement effect of CeO_2. It has been reported in the literature that the grain refinement can improve the adhesion of the oxide scale by relieving the growth and thermal stresses, resulting in the reduction of oxide spallation (Ref 42-44).

The XRD analysis (Fig. 5) of bare superalloy after hot-corrosion studies indicates the presence of Cr_2O_3, Fe_2O_3, NiO, $NaVO_3$, and TiO_2 phases in the oxide scale. In the temperature range of 900 °C, sodium sulfate (Na_2SO_4) and vanadium pentoxide (V_2O_5) react to form sodium meta-vanadate ($NaVO_3$) by following reaction:

$$Na_2SO_4 + V_2O_5 \rightarrow 2NaVO_3 + SO_3. \quad \text{(Eq 1)}$$

The $NaVO_3$ has relatively low melting point (630 °C) and is liquid at 900 °C. It acts as a catalyst and serves as an oxygen carrier to the base alloy through the open pores present on the surface leading to rapid oxidation of the base elements (Ref 45). Further, $NaVO_3$ dissolves protective oxides such as Cr_2O_3 as given by the Eq. (2) leading to depletion of protective oxides on the surface of the material (Ref 46).

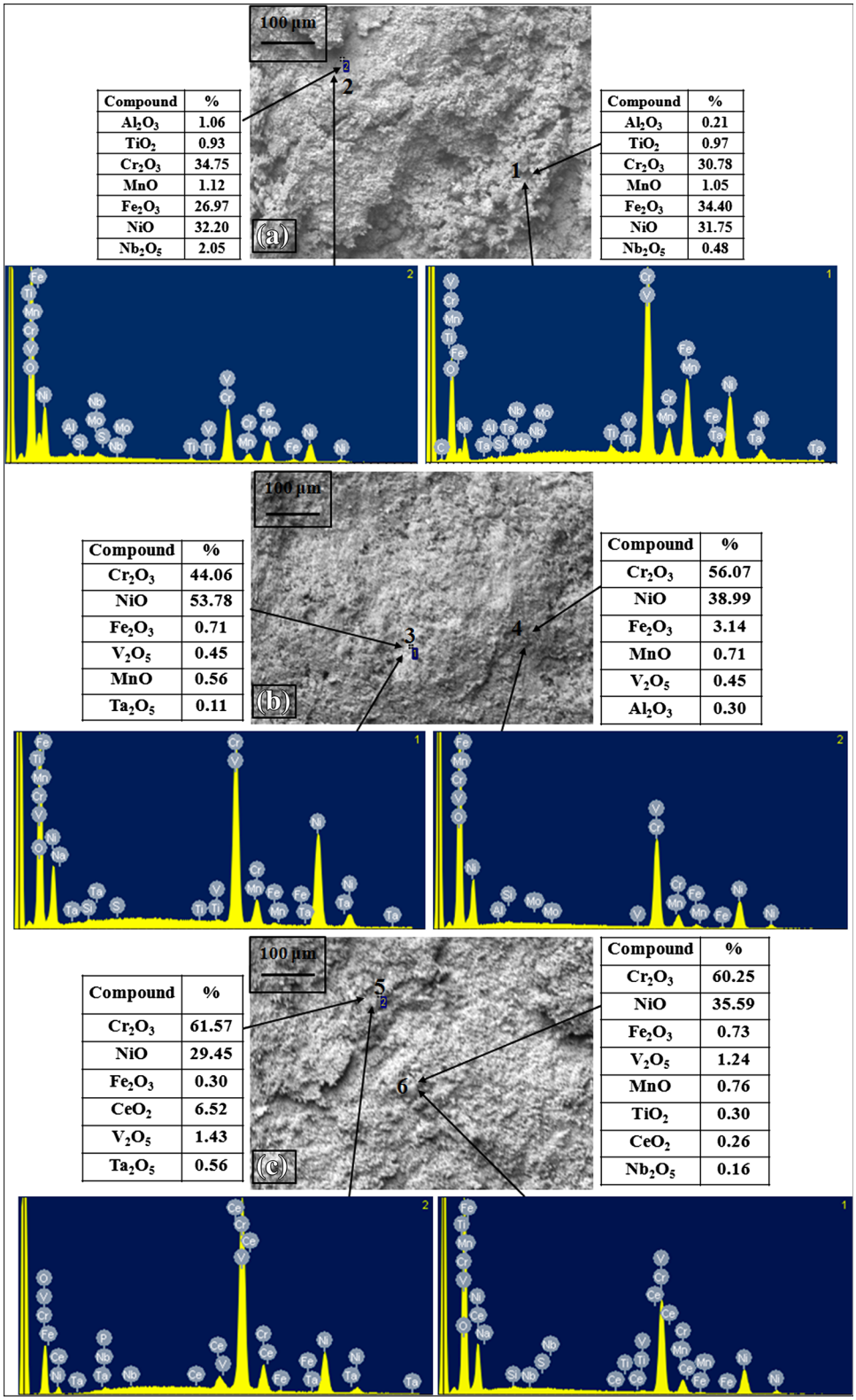

Fig. 6 Surface scale SEM/EDAX analysis of (a) bare (b) Cr_3C_2-NiCr and (c) Cr_3C_2-NiCr-CeO_2-coated superalloys subjected to hot-corrosion studies at 900 °C for 100 cycles

$$Cr_2O_3 + 4NaVO_3 + (3/2)O_2 = 2Na_2CrO_4 + 2V_2O_5. \quad \text{(Eq 2)}$$

The oxide scales of Cr_3C_2-NiCr and Cr_3C_2-NiCr-CeO_2 coatings indicate the presence of Cr_2O_3, NiO, $NiCr_2O_4$, Cr_3C_2, $Cr_{23}C_6$, and Fe_2O_3. The CeO_2 phase was observed in case of Cr_3C_2-NiCr-CeO_2 coating. Matthews et al. (Ref 47) have reported that, in oxidizing environment, Cr_3C_2 undergoes

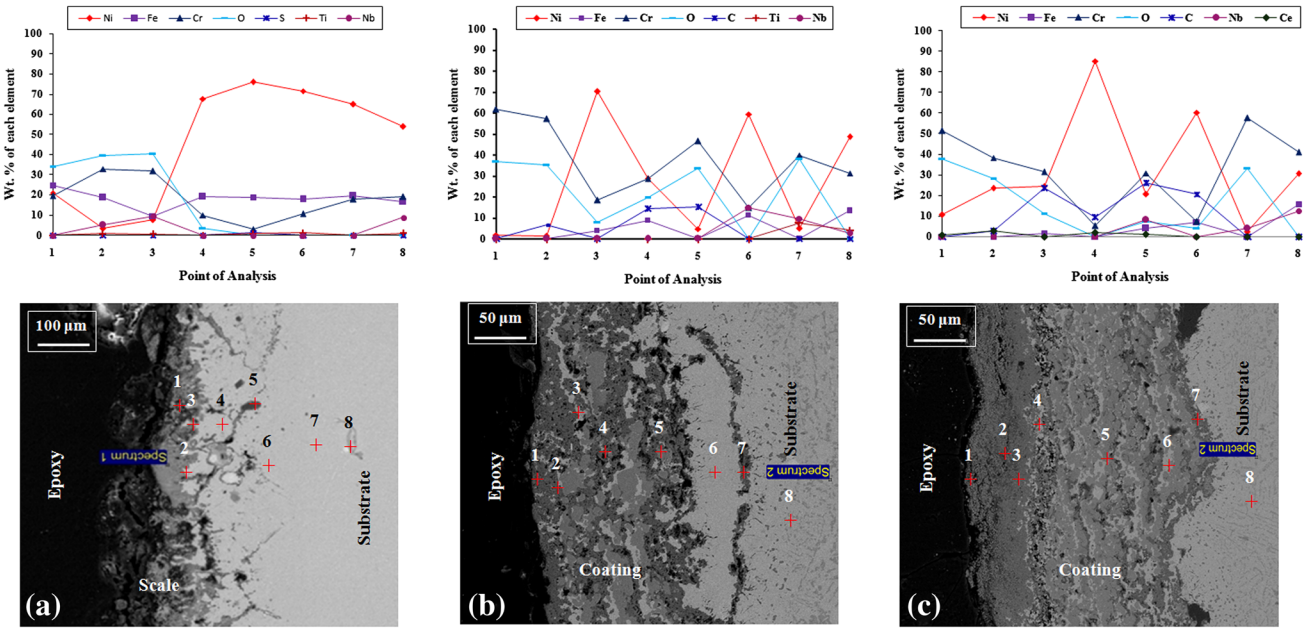

Fig. 7 Oxide scale morphology and variation of elemental composition across the cross section of (a) bare (b) Cr_3C_2-NiCr and (c) Cr_3C_2-NiCr-CeO_2-coated superalloys subjected to hot-corrosion studies at 900 °C for 100 cycles

multiple decarburization reactions to form Cr_2O_3 and carbon is removed as gaseous CO, through the following equations:

$$\begin{aligned} &+ O_2 + O_2 + O_2 + O_2 \\ &Cr_3C_2 \rightarrow Cr_7C_3 \rightarrow Cr_{23}C_6 \rightarrow [Cr_{MET}] \rightarrow Cr_2O_3, \end{aligned} \quad \text{(Eq 3)}$$

Further, Ni and O react in high-temperature oxidizing environment to form NiO and NiO in turn reacts with Cr_2O_3 to form $NiCr_2O_4$ spinel through the following reactions (Ref 48):

$$Ni + (1/2)\, O_{2(g)} = NiO_{(s)}, \quad \text{(Eq 4)}$$

$$NiO_{(s)} + Cr_2O_{3(s)} = NiCr_2O_{4(s)}. \quad \text{(Eq 5)}$$

The formation of $NiCr_2O_4$ spinel enhances hot-corrosion resistance of the coating due to their much smaller diffusion coefficient of the cations and anions than those in their parent oxides. This in turn stabilizes the metal chemistry and prevents the dissolution of the protective oxide scale (Ref 13, 47, 49). The presence of Fe_2O_3 phase on the surface of Cr_3C_2-NiCr and Cr_3C_2-NiCr-CeO_2 coatings indicates the diffusion of Fe from the substrate during hot-corrosion studies (Ref 19).

The surface EDAX analysis of bare superalloy indicates the presence of Cr_2O_3, NiO, and Fe_2O_3 as main phases. At temperatures above 700 °C, V_2O_5 dissolves the products of oxidation to form low melting eutectics, namely V_2O_5-Cr_2O_3-Fe_2O_3 (m.p 480 °C) and NiO-V_2O_5-Cr_2O_3 (m.p 550 °C). Upon cooling to lower temperatures Fe_2O_3 and Cr_2O_3 precipitate from the liquid phase and the presence of various phases in a thin layer of scale would impose such severe strain on the film that results in cracking and exfoliation of oxide scale (Ref 2, 42, 50, 51). The percentage of Fe_2O_3 at points 1 and 2 (Fig. 6a) are 34.4 and 26.97, respectively. The Fe_2O_3 is reported to be porous, non-protective oxide scale and might have allowed the penetration of corrosive species through the scale. Further, the percentage of protective Cr_2O_3 oxide phase on bare superalloy is lower when compared to Cr_3C_2-NiCr and Cr_3C_2-NiCr-CeO_2 coatings (points 1-6). The higher percentage of Fe_2O_3 present on the oxide scale may be one of the reasons for the low resistance of bare superalloy in hot-corrosion environment. The Cr_3C_2-NiCr-CeO_2 coating has highest percentage of Cr_2O_3 on the surface scale. It has been reported that addition of Ce improves the oxidation resistance of alloys due to selective oxidation of Cr and the formation of a continuous, fine-grained Cr_2O_3 scale (Ref 52). The Cr_2O_3 is thermodynamically stable up to high temperatures due to its high m.ps. It forms a dense, continuous and adherent layer that grows relatively slowly and acts as a solid diffusion barrier that inhibits interaction of corrosive species with underlying coating. Further, points 5 and 6 indicate the presence of CeO_2 on the top scale, CeO_2 has a very high free energy of formation and is very stable even at high temperatures and thus it might have blocked the diffusion of corrosive species through inter-splat regions.

The cross-sectional EDAX analysis of bare, Cr_3C_2-NiCr and Cr_3C_2-NiCr-CeO_2-coated superalloys subjected to hot-corrosion tests is shown in Fig. 7. The bare superalloy has suffered extensively due to hot-corrosion attack. The top scale of bare superalloy (points 1 and 2) shows relatively higher percentage of Fe, Cr, and Ni along with O, indicating the formation Fe_2O_3, Cr_2O_3, NiO. Oxygen has penetrated (points 1-3) into the superalloy (Fig. 7a). Also, point 5 indicates the presence of sulfur underneath the subscale region thereby indicating the porous and non protective nature of the oxide scale formed on the bare superalloy. Kamal et al. (Ref 10) has also reported the penetration of sulfur into the superalloy exposed to Na_2SO_4-60% V_2O_5 molten salt environment. The top scale of Cr_3C_2-NiCr coatings mainly shows the presence of Cr and O indicating the formation of Cr_2O_3. On the other hand top scale of Cr_3C_2-NiCr-CeO_2 coating shows the presence of Cr along with O, Ni, and C indicating the formation of oxides and carbides such as Cr_2O_3, $NiCr_2O_4$, NiO, Cr_3C_2, Cr_7C_3, and $Cr_{23}C_6$. Both Cr_3C_2-NiCr and Cr_3C_2-NiCr-CeO_2 coatings show Cr-rich dark gray and Ni-rich light gray regions in the subscale

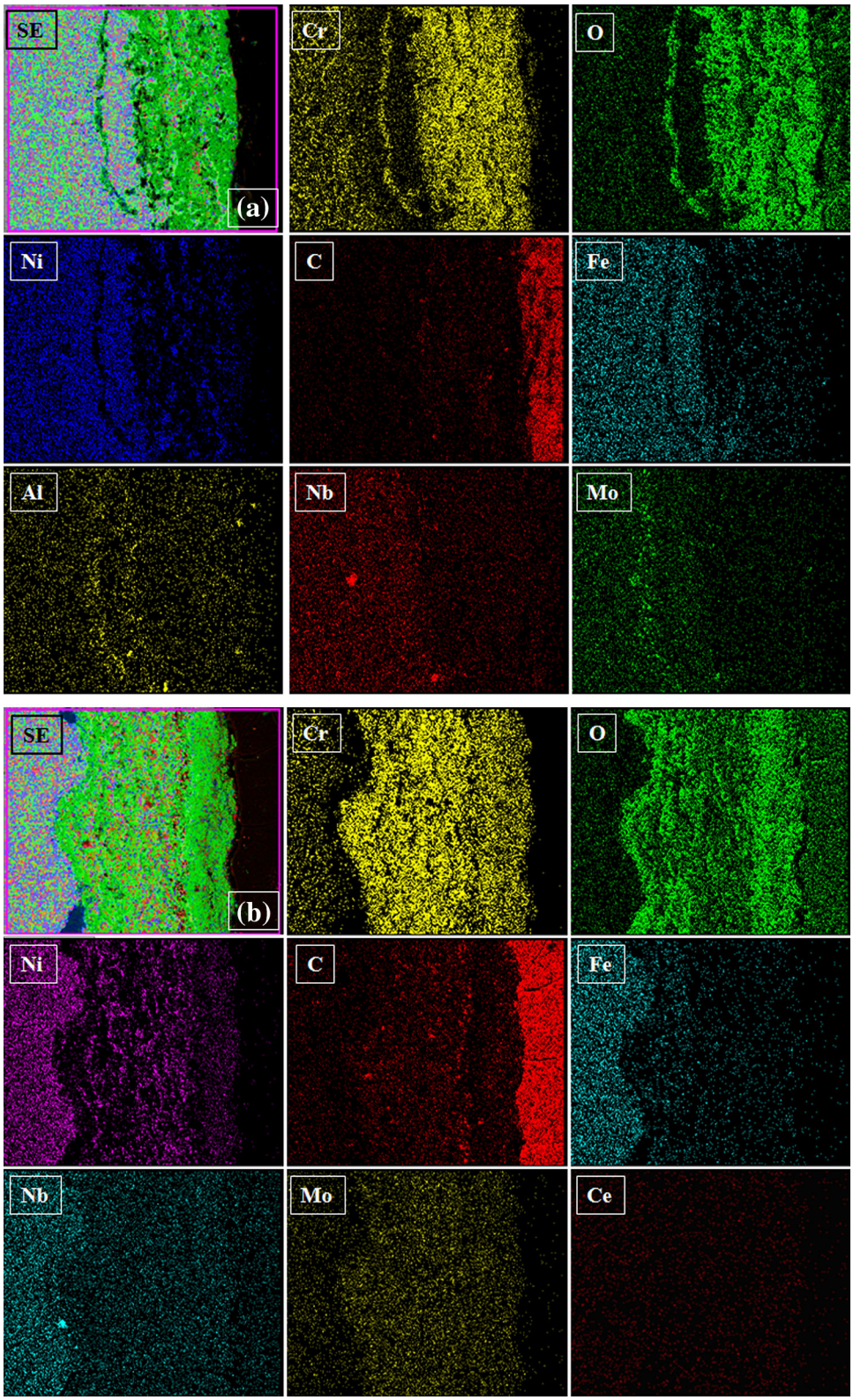

Fig. 8 Compositional image and EDX mapping of the cross section of (a) Cr_3C_2-NiCr and (b) Cr_3C_2-NiCr-CeO_2-coated superalloys subjected to hot-corrosion studies at 900 °C for 100 cycles

region. The diffusion of oxygen into subscale region of Cr_3C_2-NiCr-CeO_2 coating is negligible in comparison to that of Cr_3C_2-NiCr coating, thereby indicating the as-sprayed nature of the coating. This is further supported by EDX mapping analysis. Cr_3C_2-NiCr-CeO_2 coating shows the presence of small amount of Ce on the top scale and sub scale region. The presence of Ce in top scale is also confirmed by XRD and EDAX analysis. The presence of ceria on the top scale might

have assisted the formation of continuous, fine-grained Cr_2O_3 scale. Also, it is evident from Fig. 7 that the porosity of Cr_3C_2-NiCr-CeO_2 coating is less in comparison to that of Cr_3C_2-NiCr coating. CeO_2 is a surface-active element and it reduces the surface tension and the interfacial energy between the crystal nucleus and the melt during the process of solidification, thereby improving wetting of the surface by the coating material, which leads to better coating adhesion (Ref 31, 32). This may be the reason for reduced porosity in Cr_3C_2-NiCr-CeO_2 coating. The dense coatings provide better hot-corrosion resistance than the porous coatings and prevent short circuit transport of the reactants (Ref 34, 53). Therefore, this may be one of the reasons for the better hot-corrosion resistance of Cr_3C_2-NiCr-CeO_2 coating.

It is noticed from EDX mapping analysis of Cr_3C_2-NiCr and Cr_3C_2-NiCr-CeO_2 coatings that they are partially oxidized near the top scale (Fig. 8), where Cr, Ni, O, and C coexist indicating the formation of Cr_2O_3, $NiCr_2O_4$, NiO, Cr_3C_2, Cr_7C_3, and $Cr_{23}C_6$ phases. Also, it is clear from Fig. 8(b) that Ce is present near the inter-splat region of Cr_3C_2-NiCr-CeO_2 coating. The presence of Ce near inter-splat region might have contributed to the better adhesion of the oxide scale to the coating and thus enhanced the performance of coating in the given environment. Due to the improved adhesion between the scale and alloy, the chromium oxide that has formed along the splat boundaries might have clogged the diffusion of corrosive species into the substrate material (Ref 53). Further, from Fig. 8 we can see that, Fe is like a diffusion tracer, the diffusion of Fe from the substrate material into Cr_3C_2-NiCr-CeO_2 coating (Fig. 8b) is very little in comparison to the Cr_3C_2-NiCr coating (Fig. 8a). Therefore, the Cr_3C_2-NiCr-CeO_2 coating has slower diffusion coefficient, leading to slower scale growth.

Finally, based on present investigation, it can be inferred that Cr_3C_2-NiCr-CeO_2 coating has provided better hot-corrosion resistance in the given environment when compared with bare and Cr_3C_2-NiCr-coated superalloys.

5. Conclusions

The hot-corrosion behavior of D-gun sprayed Cr_3C_2-NiCr-CeO_2 coating on Ni-based superalloy Inconel 718 has been studied and the following conclusions were made.

1. The addition of CeO_2 has enhanced the hot-corrosion resistance of D-gun sprayed Cr_3C_2-NiCr coating in Na_2SO_4-60%V_2O_5 molten salt environment.
2. The addition of CeO_2 has effectively improved the micro-hardness, porosity, and surface roughness values of Cr_3C_2-NiCr coating.
3. The formation of Cr_2O_3, $NiCr_2O_4$, and NiO on the top scale, along with the presence of CeO_2 at the inter-splat regions of Cr_3C_2-NiCr-CeO_2 has provided better protection to the substrate material. The formations of these oxides are confirmed by XRD, EDAX, and EDX mapping.
4. The addition of CeO_2 has contributed to selective oxidation of chromium to form Cr_2O_3. It has also contributed to better adhesion of the oxide scale with the coating and thus enhanced the performance of coating in the given environment. The presence of cerium oxide is confirmed by XRD, EDAX, and EDX mapping analysis.
5. The formation of Cr_2O_3 due to successive decarburization of Cr_3C_2 has been indicated by XRD analysis.
6. Small amount of oxides of iron, silicon, manganese, titanium, and niobium were present on the top scale of the coated samples indicating the diffusion of these elements from the substrate material.

Acknowledgment

The authors would like to thank Dr. Mukul Gupta of UGC-DAE Consortium for Scientific Research, Indore for performing XRD analysis. The authors also wish to thank Mr. Hiren Upadhyay and Mr. Sagar Jagtap of SIC, SVNIT, Surat for performing SEM/EDAX analysis.

References

1. H. Singh, S. Prakash, D. Puri, and D.M. Phase, Cyclic Oxidation Behavior of Some Plasma-Sprayed Coatings in Na_2SO_4-60%V_2O_5 Environment, *J. Mater. Eng. Perform.*, 2006, **15**(6), p 729–741
2. H. Singh, D. Puri, and S. Prakash, An Overview of Na_2SO_4 And/Or V_2O_5 Induced Hot Corrosion of Fe- and Ni-Based Superalloys, *Rev. Adv. Mater. Sci.*, 2007, **16**, p 27–50
3. S. Saladi, J. Menghani, and S. Prakash, Hot Corrosion Behaviour of Detonation-Gun Sprayed Cr_3C_2-NiCr Coating on Inconel-718 in Molten Salt Environment at 900 °C, *Trans. Indian Inst. Met.*, 2014, **67**(5), p 623–627
4. N. Eliaz, G. Shemesh, and R.M. Latannision, Hot Corrosion in Gas Turbine Components, *Eng. Fail. Anal.*, 2002, **9**, p 31–43
5. Lin Geng, Young-Sang Na, and Nho-Kwang Park, Oxidation Behavior of Alloy 718 at a High Temperature, *Mater. Des.*, 2007, **28**, p 978–981
6. J. Sekar Saladi and S.Prakash Menghani, A Study on the Cyclic Oxidation Behaviour of Detonation-Gun-Sprayed Ni-5Al Coatings on Inconel-718 at 900 °C, *J. Mater. Eng. Perform*, 2014, **23**(12), p 4394–4403
7. S. Kamal, R. Jayaganthan, and S. Prakash, High Temperature Cyclic Oxidation And Hot Corrosion Behaviours of Superalloys at 900 °C, *Bull. Mater. Sci.*, 2010, **33**(3), p 299–306
8. T.S. Sidhu, R.D. Agrawal, and S. Prakash, Hot Corrosion of Some Superalloys and Role of High-Velocity Oxy-Fuel Spray Coatings—A Review, *Surf. Coat. Technol.*, 2005, **198**, p 441–446
9. T.S. Sidhu, S. Prakash, and R.D. Agrawal, Characterizations and Hot Corrosion Resistance of Cr_3C_2-NiCr Coating on Ni-Base Superalloys in an Aggressive Environment, *J. Therm. Spray Technol.*, 2006, **15**(4), p 811–816
10. S. Kamal, R. Jayaganthan, S. Prakash, and S. Kumar, Hot Corrosion Behaviour of Detonation Gun Sprayed Cr_3C_2-NiCr Coatings on Ni and Fe-Based Superalloys in Na_2SO_4-60% V_2O_5 Environment at 900 °C, *J. Alloys Compd.*, 2008, **463**, p 358–372
11. T.S. Sidhu, S. Prakash, and R.D. Agrawal, Hot Corrosion Resistance of High-Velocity Oxyfuel Sprayed Coatings on a Nickel-Base Superalloy in Molten Salt Environment, *J. Therm. Spray Technol.*, 2006, **15**(3), p 387–399
12. T.S. Sidhu, S. Prakash, and R.D. Agrawal, A Comparative Study of Hot Corrosion Resistance of HVOF Sprayed NiCrBSi and Stellite-6 Coated Ni-Based Superalloy at 900 °C, *Mater. Sci. Eng. A*, 2007, **445–446**, p 210–218
13. M. Kaur, H. Singh, and S. Prakash, Surface Engineering Analysis of Detonation-Gun Sprayed Cr_3C_2-NiCr Coating Under High-Temperature Oxidation and Oxidation–Erosion Environments, *Surf. Coat. Technol.*, 2011, **206**, p 530–541
14. M.H. Staia, T. Valente, C. Bartuli, D.B. Lewis, and C.P. Constable, Characterization of Cr_3C_2-25% NiCr Reactive Plasma Sprayed Coatings Produced at Different Pressures, *Surf. Coat. Technol.*, 2001, **146–147**, p 553

15. B. Yin, G. Liu, H. Zhou, J. Chen, and F. Yan, Sliding Wear Behavior of HVOF-sprayed Cr3C2–NiCr/CeO2 Composite Coatings at Elevated Temperature up to 800 C, *Tribol. Lett.*, 2010, **37**, p 463–475
16. J. Wang, L. Zhang, B. Sun, and Y. Zhou, Study of the Cr_3C_2-NiCr Detonation Spray Coating, *Surf. Coat. Technol.*, 2000, **130**(1), p 69–73
17. T.S. Sidhu, S. Prakash, and R.D. Agrawal, Evaluation of Hot Corrosion Resistance of HVOF Coatings on a Ni-Based Superalloy in Molten Salt Environment, *Mater. Sci. Eng. A*, 2006, **430**(1–2), p 64–78
18. Z. Zhang, X. Lu, and J. Luo, Tribological Properties of Rare Earth Oxide Added Cr_3C_2-NiCr Coatings, *Appl. Surf. Sci.*, 2007, **253**, p 4377–4385
19. R. Subhash Kamal and S.Prakash Jayaganthan, High Temperature Oxidation Studies of Detonation-Gun-Sprayed Cr_3C_2-NiCr Coating on Fe- and Ni-Based Superalloys in Air Under Cyclic Condition at 900 °C, *J. Alloys Compd.*, 2009, **472**, p 378–389
20. C. Senderowski and Z. Bojar, Gas Detonation Spray Forming of Fe-Al Coatings in the Presence of Interlayer, *Surf. Coat. Technol.*, 2008, **202**(15), p 3538–3548
21. Cezary Senderowski and Z. Bojar, Influence of Detonation Gun Spraying Conditions on the Quality of Fe-Al Intermetallic Protective Coatings in the Presence of NiAl and NiCr Interlayers, *J. Therm. Spray Technol.*, 2009, **18**(3), p 435–447
22. C. Senderowski, Z. Bojar, W. Wołczyński, and A. Pawłowski, Microstructure Characterization of D-Gun Sprayed Fe-Al Intermetallic Coatings, *Intermetallics*, 2010, **18**(7), p 1405–1409
23. C. Senderowski, Nanocomposite Fe-Al Intermetallic Coating Obtained by Gas Detonation Spraying of Milled Self-Decomposing Powder, *J. Therm. Spray Technol.*, 2014, **23**(7), p 1124–1134
24. C. Senderowski, D. Zasada, T. Durejko, and Z. Bojar, Characterization of As-Synthesized and Mechanically Milled Fe-Al Powders Produced by the Self-Disintegration Method, *Powder Technol.*, 2014, **263**, p 96–103
25. C. Senderowski, A. Pawłowski, Z. Bojar, W. Wołczyński, M. Faryna, J. Morgiel, and Ł. Major, TEM Microstructure of Fe-Al Coatings Detonation Sprayed onto Steel Substrate, *Arch. Metall. Mater.*, 2010, **55**(2), p 373–381
26. G. Sundararajan, K.U.M. Prasad, D.S. Rao, and S.V. Joshi, A Comparative Study of Tribological Behaviour of Plasma and D-Gun Sprayed Coatings under Different Wear Modes, *J. Mater. Eng. Perform.*, 1998, **7**(3), p 343–351
27. R.A. Rapp, J.H. Devan, D.L. Douglass, P.C. Nordine, F.S. Pettit, and D.P. Whittle, High Temperature Corrosion in Energy Systems, *Mater. Sci. Eng.*, 1981, **50**, p 1–17
28. B. Yin, G. Liu, H. Zhou, J. Chen, and F. Yan, Microstructures and Properties of Plasma Sprayed FeAl/CeO_2/ZrO_2 Nano-Composite Coating, *Appl. Surf. Sci.*, 2010, **256**, p 4176–4184
29. Y. Wang, J.J. Liu, and Z.H. Yu, Effect of Rare Earth Elements on Microstructure and Wear Resistance of Laser Remelted Iron Alloy Coatings Containing Metalloids, *Surf. Eng.*, 1993, **9**, p 151–153
30. Y. Wang, Z.H. Yu, J.J. Liu, C.S. Wang, and Q.A. Li, The Influence of CeO_2 on the Microstructure and Wear Resistance of M80S20 Flame Spray and Flame Spray Welding Coatings, *J. Rare Earths*, 1992, **10**, p 212–216
31. Y. Wang, Z. Wang, Y. Yang, and W. Chen, The Effects of Ceria on the Mechanical Properties and Thermal Shock Resistance of Thermal Sprayed NiAl Intermetallic Coatings, *Intermetallics*, 2008, **16**(5), p 682–688
32. S. Kamal, R. Jayaganthan, and S. Prakash, Hot Corrosion Studies of Detonation-Gun-Sprayed NiCrAlY + 0.4 wt.% CeO_2 Coated Superalloys in Molten Salt Environment, *J. Mater. Eng. Perform.*, 2011, **20**(6), p 1068–1077
33. R.A. Mahesh, G. Rao, R. Jayaganthan, and S. Prakash, Hot Corrosion Behaviour of HVOF Sprayed NiCrAlY-0.4 wt.%CeO_2 Coatings on Superalloys in Aggressive Environment at 900 °C, *Corros. Eng. Sci. Technol.*, 2010, **45**(2), p 142–149
34. S. Kamal, R. Jayaganthan, and s Prakash, Mechanical and Microstructural Characteristics of Detonation Gun Sprayed NiCrAlY + 0.4 wt.% CeO_2 Coatings on Superalloys, *Mater. Chem. Phys.*, 2010, **122**, p 262–268
35. X. Gui-hua, W. Guo-feng, and Z. Kai-feng, Effect of Rare Earth Y on Oxidation Behavior of NiAl-Al_2O_3, *Trans. Nonferr. Met. Soc. China*, 2011, **21**, p s362–s368
36. Z. Xu, L. He, R. Mu, S. He, G. Huang, and X. Cao, Hot Corrosion Behavior of Rare Earth Zirconates and Yttria Partially Stabilized Zirconia Thermal Barrier Coatings, *Surf. Coat. Technol.*, 2010, **204**, p 3652–3661
37. S. Saladi, J. Menghani, and S. Prakash, A Study on the Cyclic Oxidation Behavior of Detonation-Gun-Sprayed Ni-5Al Coatings on Inconel-718 at 900 °C, *J. Mater. Eng. Perform.*, 2014, **23**, p 4394–4403
38. Sekar Saladi, J. Menghani, and S. Prakash, High Temperature Oxidation Behaviour of Detonation-Gun-Sprayed Cr_3C_2-NiCr-CeO_2 Coatings on Inconel-718 at 900 °C, *ASME Turbo Expo*, ASME, 2014
39. Z. Zhang, X. Lu, B. Han, and J. Luo, Rare Earth Effect on Microstructure, Mechanical and Tribological Properties of CoCrW Coatings, *Mater. Sci. Eng. A*, 2007, **444**(1–2), p 92–98
40. R.A. Mahesh, R. Jayaganthan, and S. Prakash, Oxidation Behavior of HVOF Sprayed Ni-5Al Coatings Deposited on Ni- and Fe-Based Superalloys Under Cyclic Condition, *Mater. Sci. Eng. A*, 2008, **475**(1–2), p 327–335
41. H. Choi, B. Yoon, H. Kim, and C. Lee, Isothermal Oxidation of Air Plasma Spray NiCrAlY Bond Coatings, *Surf. Coat. Technol.*, 2002, **150**(2–3), p 297–308
42. G. Goyal, H. Singh, and S. Prakash, Effect of Superficially Applied ZrO_2 Inhibitor on the High Temperature Corrosion Performance of Some Fe-, Co- and Ni-Base Superalloys, *Appl. Surf. Sci.*, 2008, **254**(20), p 6653–6661
43. Gao-Min Zhao and K.-L. Wang, Effect of La_2O_3 on Resistance to High-Temperature Oxidation of Laser Clad Ferrite-Based Alloy Coatings, *Surf. Coat. Technol.*, 2005, **190**, p 249–254
44. Y.M. Zhang, M. Hida, H. Hashimoto, Z.P. Luo, and S.X. Wang, Effect of Rare-Earth Oxide (CeO_2) on the Microstructures in Laser Melted Layer, *J. Mater. Sci.*, 2000, **35**, p 5389–5400
45. R.A. Mahesh, R. Jayaganthan, and S. Prakash, A Study on Hot Corrosion Behaviour of Ni-5Al Coatings on Ni- and Fe-Based Superalloys in an Aggressive Environment at 900 °C, *J. Alloys Compd.*, 2008, **460**(1–2), p 220–231
46. J. Swaminathan, S. Raghavan, and S.R. Iyer, Studies on the Hot Corrosion of Some Nickel-Base Superalloys by Vanadium Pentoxide, *Trans. Indian Inst. Met.*, 1993, **46**(3), p 175–181
47. S. Matthews, B. James, and M. Hyland, High Temperature Erosion–Oxidation of Cr_3C_2-NiCr Thermal Spray Coatings Under Simulated Turbine Conditions, *Corros. Sci.*, 2013, **70**, p 203–211
48. W.H. Lee and R.Y. Lin, Hot Corrosion Mechanism of Intermetallic Compound Ni_3Al, *Mater. Chem. Phys.*, 2002, **77**, p 86–96
49. S. Kamal, R. Jayaganthan, and S. Prakash, Evaluation of Cyclic Hot Corrosion Behaviour of Detonation Gun Sprayed Cr_3C_2-NiCr Coatings on Ni- and Fe-Based Superalloys, *Surf. Coat. Technol.*, 2009, **203**, p 1004–1013
50. K. Sachs, Accelerated High Temperature Oxidation Due to Vanadium Pentoxide, *Metallurgia, Apr.*, 1958, p. 167-173
51. S.R. Iyer, K.J.L. Iyer, and V.M. Radhakrishan, High Temperature Corrosion of a Ni-Base Superalloy by Vanadium, *Proc. of 10th ICMC, IV*, 1987, p. 3665
52. P. Papaiacovou, R.J. Hussey, D.F. Mitchell, and M.J. Graham, The Effect of CeO_2 Coatings on the Oxidation Behaviour of Fe-20Cr Alloys in O_2 at 1173 K, *Corros. Sci.*, 1990, **30**(4–5), p 451–455
53. R.A. Mahesh, R. Jayaganthan, and S. Prakash, A Study on The Oxidation Behaviour of HVOF Sprayed NiCrAlY-0.4 wt.% CeO_2 Coatings on Superalloys at Elevated Temperature, *Mater. Chem. Phys.*, 2010, **119**, p 449–457